



Bulky dendritic triarylamine-based organic dyes for efficient co-adsorbent-free dye-sensitized solar cells

Yong Hua^{a,b}, Bin Jin^c, Hongda Wang^{a,b}, Xunjin Zhu^{a,b,*}, Wenjun Wu^{c,**}, Man-Sing Cheung^d, Zhenyang Lin^d, Wai-Yeung Wong^{a,b,*}, Wai-Kwok Wong^{a,b,*}

^a Institute of Molecular Functional Materials, Department of Chemistry and Institute of Advanced Materials, Hong Kong Baptist University, Waterloo Road, Kowloon Tong, Hong Kong, China

^b HKBU Institute of Research and Continuing Education, Shenzhen Virtual University Park, Shenzhen 518057, PR China

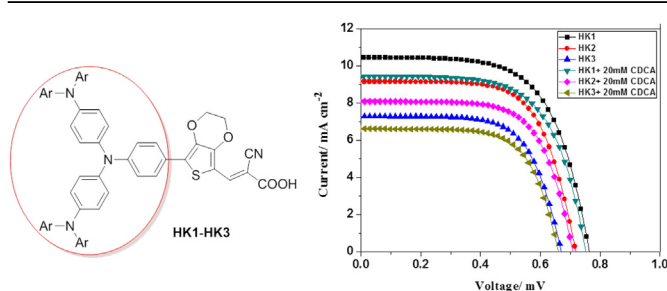
^c Key Laboratory for Advanced Materials and Institute of Fine Chemicals, East China University of Science and Technology, Meilong Road 130, Shanghai 200237, PR China

^d Department of Chemistry, The Hong Kong University of Science and Technology, Clearwater Bay, Hong Kong, China

HIGHLIGHTS

- New organic dyes with bulky dendritic electron-donating groups were synthesized.
- The structural characteristics can effectively suppress dye aggregation in DSSCs.
- The PCEs of DSSCs are significantly decreased in the presence of the co-adsorbent.

GRAPHICAL ABSTRACT



ARTICLE INFO

Article history:

Received 9 January 2013
Received in revised form
26 February 2013
Accepted 2 March 2013
Available online 15 March 2013

Keywords:

Triarylamine derivatives
Dendrimers
Dye-sensitized solar cells
Co-adsorbent-free
Aggregation

ABSTRACT

Three new organic photosensitizers (**HK1–HK3**) incorporating functionalized bulky trimer of triarylamine derivatives as the electron donor units, 3,4-ethylenedioxythiophene moiety as the conjugated spacer, and cyanoacrylic acid as the electron acceptor, have been synthesized and the effects of different bulky electron donor substituents on the photovoltaic performances of dye-sensitized solar cells (DSSCs) are investigated accordingly. The DSSC based on **HK1** with tris(triphenylamine) electron donor in the absence of the co-adsorbent chenodeoxycholic acid (CDCA) shows the best photovoltaic performance under standard global AM 1.5 sunlight: a short-circuit current density (J_{sc}) of 10.41 mA cm⁻², an open-circuit voltage of 0.76 V and a fill factor of 0.65, corresponding to a maximum overall power conversion efficiency (PCE) of 5.11%. However, in the presence of co-adsorbent CDCA, the PCEs of DSSCs based on these photosensitizers, decrease significantly by about 9.7%, which is contrary to the conventional concept that CDCA can improve the efficiency by inhibition of dye aggregation and intermolecular electron recombination. The results demonstrate that the synthesized new organic dyes with bulky dendritic triarylamine and its derivatives as electron-donation units can efficiently suppress dye aggregation without the need of the co-adsorbent and effectively reduce the intramolecular electron recombination in DSSCs.

© 2013 Elsevier B.V. All rights reserved.

* Corresponding authors. Institute of Molecular Functional Materials, Department of Chemistry and Institute of Advanced Materials, Hong Kong Baptist University, Waterloo Road, Kowloon Tong, Hong Kong, China. Tel.: +852 34115157; fax: +852 3411 7348.

** Corresponding author. Fax: +86 21 64252756.

E-mail addresses: xjzhu@hkbu.edu.hk (X. Zhu), bulinton@163.com (W. Wu), rwywong@hkbu.edu.hk (W.-Y. Wong), wk Wong@hkbu.edu.hk (W.-K. Wong).

1. Introduction

In the past two decades, dye-sensitized solar cells (DSSCs) based on nanocrystalline porous TiO_2 have attracted intense attention since the seminal report by Grätzel and co-workers for the low material cost compared with conventional inorganic silicon-based solar cells [1]. Generally, a typical DSSC consists of three main components: a wide band gap TiO_2 semiconductor deposited on a transparent conducting glass substrate, an anchored molecular sensitizer, and a redox electrolyte/hole transporter [2–6]. Among the three key components, the sensitizer always plays the most crucial role since it exerts a significant influence on the power conversion efficiency (PCE) of light to electricity, as well as the device stability. Initially, DSSCs based on ruthenium(II) polypyridyl sensitizers, such as N3 [7], N719 [8] and black dye [9] have achieved PCEs above 11% under standard AM 1.5 solar light irradiation. However, the high cost of the precious ruthenium metal and synthetic difficulties for ruthenium(II) complexes tends to limit their further development for large-scale application. Therefore a variety of metal-free organic photosensitizers have been developed and applied in DSSCs due to their high molar extinction coefficient, simple preparation procedures and low cost. Up to now, the solar-cell performances of DSSCs based on pure organic dyes have reached impressive efficiencies in the range of 5–9.7% [10–18]. And most organic sensitizers applied in highly efficient solar cells follow a donor– π -spacer–acceptor (D– π -A) configuration. However, the structural features of these organic sensitizers may facilitate the dye aggregation on the semiconductor surface and electron recombination with the triiodide ions present in the electrolyte [19–21]. In order to avoid these unfavorable dye aggregation and electron recombination and obtain optimal solar-cell performance, an appropriate nonplanar structural moiety can be introduced into the organic framework. Recently, Ko et al. reported a novel triphenylamine dye containing a nonplanar bis-dimethylfluorenylamino unit with a PCE of 7.2% [22]. Tian et al. have also designed a series of novel starburst triarylamine-based organic dyes, which can effectively inhibit aggregation between molecules and enhance the stability of the solar cells, yielding 6.02% power conversion efficiency [23]. Notably, simple organic dyes that contain common triphenylamine (TPA) as donor and cyanoacrylic acid as electron acceptor (and anchoring group), in which those two moieties are bridged by thiophene and its derivatives, have been demonstrated to show good performance in DSSCs in the presence of deoxycholic acid (DCA) as a coadsorbate. With the notion of incorporating an additional nonplanar triarylamine moiety into these simple organic frameworks, we expect the absorption region can be extended in the resulting D–D– π -A structure, and the molar extinction coefficient can also be enhanced as compared to the D– π -A structure. Moreover, they benefit from the lower tendency to aggregate and better thermo-stability [24–26].

Here, we have designed and synthesized three new organic photosensitizers (**HK1**, **HK2** and **HK3**) containing bulky rigid trimers of triarylamine derivatives as the donor group and cyanoacrylic acid as an electron acceptor, in which these two moieties are bridged with 3,4-ethylenedioxythiophene (EDOT) as shown in Fig. 1. The photophysical and electrochemical properties of the three dyes and their photovoltaic performances of the DSSCs have been studied by UV–visible absorption spectroscopy, cyclic voltammetry (CV), density functional theory (DFT) and electrochemical impedance spectroscopy (EIS). The results demonstrate that the three dyes favor light harvesting, prevent dye aggregation and suppress the dark current significantly in DSSCs, leading to attractive performance even in the absence of the co-adsorbent chenodeoxycholic acid (CDCA).

2. Experimental section

2.1. Materials and characterization

All solvents and chemicals were purchased from Sigma–Aldrich Company and used without further purification. 7-Bromo-2,3-dihydrothieno[3,4-*b*] [1,4]dioxine-5-carbaldehyde (**1**) [27], *N,N*-diphenyl-4-(4,4,5,5-tetramethyl-1,3,2-dioxaborolan-2-yl) aniline (**2**), *N*-(9,9-dimethyl-9*H*-fluoren-2-yl)-9,9-dimethyl-*N*-(4-(4,4,5,5-tetramethyl-1,3,2-dioxaborolan-2-yl)phenyl)-9*H*-fluoren-2-amine (**3**), and 4-(hexyloxy)-*N*-(4-(hexyloxy)phenyl)-*N*-(4-(4,4,5,5-tetramethyl-1,3,2-dioxaborolan-2-yl)phenyl)aniline (**4**) [28], and 7-(4-(diphenylamino)phenyl)-2,3-dihydrothieno[3,4-*b*] [1,4]dioxine-5-carbaldehyde (**5**) [27] were prepared according to the literature methods reported.

^1H and ^{13}C NMR spectra were recorded with a Bruker Ultra-shield 400 Plus NMR spectrometer. The UV–visible absorption spectra of these dyes in CH_2Cl_2 solution were measured with a Varian Cary 100 UV–visible spectrophotometer. Emission spectra were performed using a Photon Technology International (PTI) Alphascan spectrofluorimeter. High-resolution matrix-assisted laser desorption/ionization time of flight (MALDI-TOF) mass spectra were obtained with a Bruker Autoflex MALDI-TOF mass spectrometer. The cyclic voltammograms (CV) were measured with Versastat II electrochemical work station using a normal three-electrode cell with a Pt working electrode, a Pt wire counter electrode and an Ag/AgCl reference electrode. The supporting electrolyte was 0.1 M tetra-*n*-butylammonium hexafluorophosphate ($^n\text{Bu}_4\text{NPF}_6$) in THF. Ferrocene was added as a calibrant after each set of measurements, and all potentials reported were quoted with reference to ferrocene-ferrocenium (Fc^+/Fc) couple (taken as $E_{1/2} = +0.27$ V relative to the reference electrode). The highest occupied molecular orbital (HOMO) was deduced by the equation $E_{\text{HOMO}} = -(E_{\text{ox}} + 4.80)$ eV, assuming that the energy level of ferrocene-ferrocenium to be -4.80 eV. Estimated from the UV–visible absorption spectrum, the energy band gaps of these sensitizers were obtained. Thus, the lowest unoccupied molecular orbital (LUMO) level was calculated to be the sum of the energy band gap and the HOMO level [29].

7-(4-(Bis(4-bromophenyl)amino)phenyl)-2,3-dihydrothieno[3,4-*b*] [1,4]dioxine-5-carbaldehyde (**6**).

N-Bromosuccinimide NBS (411 mg, 2.31 mmol) was added in one portion to the solution of **5** (400 mg, 1.0 mmol) in THF (50 mL) at 0 °C. The mixture was allowed to warm to room temperature and stirring was continued for 1.5 h. Then, the reaction was quenched by the addition of water (50 mL) and extracted with CH_2Cl_2 . The collected organic layer was evaporated under vacuum and the residue was purified by column chromatography on silica gel with CH_2Cl_2 as eluent to give a yellow solid (577 mg, 98%).

^1H NMR (400 MHz, CDCl_3): δ (ppm) 9.86 (s, 1H), 7.39 (d, $J = 8.8$ Hz, 4H), 7.21 (d, $J = 8.8$ Hz, 2H), 7.13 (d, $J = 8.8$ Hz, 2H), 6.99 (d, $J = 8.8$ Hz, 4H), 4.35 (s, 2H), 4.31 (s, 2H). HRMS (MALDI-TOF) m/z : 568.9331 [M^+]; calcd for $\text{C}_{25}\text{H}_{17}\text{Br}_2\text{NO}_3\text{S}$ [M^+]: 568.9329.

The general procedure for the preparation of **7**, **8** and **9** was described below.

The mixture of **6** (100 mg, 0.18 mmol), **2** (or **3** or **4**) (150 mg, 0.40 mmol), $\text{Pd}(\text{PPh}_3)_4$ (25 mg, 0.04 mmol), 2 N aqueous solution of K_2CO_3 (2 mL) in THF (10 mL) was heated to reflux under a N_2 atmosphere for about 12 h. Then, the solvent was removed under vacuum and the residue was purified by column chromatography on silica gel using a 4:1 mixture of *n*-hexane and CH_2Cl_2 as eluent to afford the title yellow compound in about 65% yield. **7**: ^1H NMR (400 MHz, CDCl_3): δ (ppm) 9.90 (s, 1H), 7.69 (d, $J = 8.8$ Hz, 2H), 7.48 (d, $J = 8.8$ Hz, 4H), 7.44 (d, $J = 8.8$ Hz, 4H), 7.24–7.28 (m, 6H), 7.18 (d,

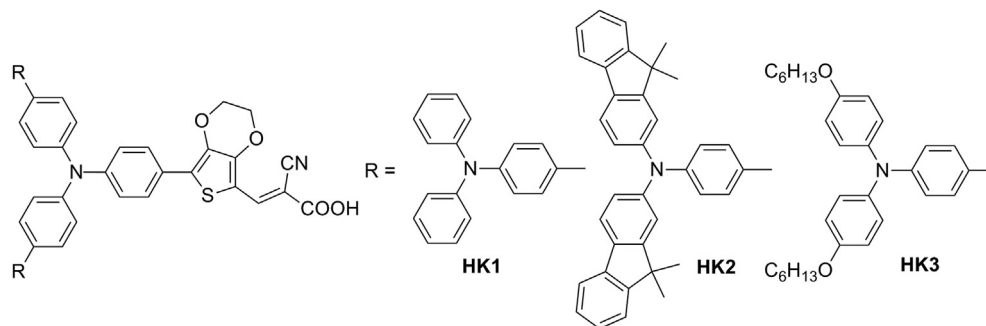


Fig. 1. Molecular structures of the new dyes **HK1**–**HK3**.

$J = 8.8$ Hz, 4H), 7.12 (m, 14H), 7.02 (t, $J = 8.8$ Hz, 6H), 4.39 (s, 2H), 4.36 (s, 2H). HRMS (MALDI-TOF) m/z : 899.3223 [M^+]; calcd for $C_{61}H_{45}N_3O_3S$ [M^+]: 899.3229.

8: 1H NMR (400 MHz, $CDCl_3$): δ (ppm) 9.91 (s, 1H), 7.68 (d, $J = 8.8$ Hz, 2H), 7.64 (d, $J = 8.8$ Hz, 4H), 7.59 (d, $J = 8.8$ Hz, 4H), 7.53 (d, $J = 8.8$ Hz, 4H), 7.49 (d, $J = 8.8$ Hz, 4H), 7.40 (d, $J = 8.8$ Hz, 4H), 7.30–7.33 (m, 6H), 7.21–7.28 (m, 12H), 7.09–7.14 (m, 8H), 4.41 (s, 2H), 4.37 (s, 2H), 1.30 (s, 24H). HRMS (MALDI-TOF) m/z : 1363.5745 [M^+]; calcd for $C_{97}H_{77}N_3O_3S$ [M^+]: 1363.5751.

9: 1H NMR (400 MHz, $CDCl_3$): δ (ppm) 9.91 (s, 1H), 7.65 (d, $J = 8.0$ Hz, 2H), 7.52 (d, $J = 8.0$ Hz, 4H), 7.43 (d, $J = 8.0$ Hz, 4H), 7.08 (m, 6H), 6.99 (d, $J = 8.0$ Hz, 8H), 6.87 (d, $J = 8.0$ Hz, 8H), 6.78 (d, $J = 8.0$ Hz, 4H), 4.42 (s, 2H), 4.36 (s, 2H), 3.90 (m, 8H), 1.68 (m, 8H), 1.28 (m, 8H), 1.14 (m, 16H), 0.86 (t, $J = 7.2$ Hz, 12H). HRMS (MALDI-TOF) m/z : 1299.6745 [M^+]; calcd for $C_{85}H_{93}N_3O_7S$ [M^+]: 1299.6751.

The three dyes **HK1**–**HK3** were prepared similarly as described below.

A mixture of precursor **7**, **8** or **9** (100 mg, 0.11 mmol) with cyanoacetic acid (89 mg, 1.10 mmol) in acetic acid (20 mL) was refluxed overnight in the presence of ammonium acetate (200 mg) under a N_2 atmosphere. Then, water was added and the organic layer extracted with CH_2Cl_2 . Next, the solvent was removed under vacuum and the crude compound was purified by column chromatography on silica gel eluting with CH_2Cl_2 and MeOH (20:1, v/v) to give a dark red solid in 61–71% yield.

HK1: 1H NMR (400 MHz, d_6 -DMSO): δ (ppm) 8.16 (s, 1H), 7.67 (d, $J = 8.0$ Hz, 2H), 7.52–7.58 (m, 8H), 7.30 (t, $J = 8.0$ Hz, 8H), 7.11 (d, $J = 8.0$ Hz, 4H), 6.98–7.07 (m, 18H), 4.46 (s, 2H), 4.37 (s, 2H). ^{13}C NMR (400 MHz, d_6 -DMSO): δ (ppm) 147.4, 146.9, 145.6, 138.0, 135.5, 133.8, 130.0, 128.3, 127.8, 127.6, 125.3, 124.5, 123.7, 123.6, 55.3. HRMS (MALDI-TOF) m/z : 966.3224 [M^+]; calcd for $C_{64}H_{46}N_4O_4S$ [M^+]: 966.3244.

HK2: 1H NMR (400 MHz, d_6 -DMSO): δ (ppm) 8.13 (s, 1H), 7.71 (t, $J = 8.0$ Hz, 9H), 7.58–7.68 (m, 10H), 7.46 (d, $J = 8.0$ Hz, 4H), 7.22–7.31 (m, 12H), 7.11–7.14 (m, 8H), 7.07 (d, $J = 8.0$ Hz, 2H), 6.99–7.02 (m, 4H), 4.44 (s, 2H), 4.38 (s, 2H), 1.33 (s, 24H). ^{13}C NMR (400 MHz, d_6 -DMSO): δ (ppm) 154.7, 153.0, 146.6, 146.4, 145.0, 138.2, 134.8, 133.7, 133.3, 127.8, 126.6, 124.9, 123.6, 122.8, 122.5, 121.0, 119.4, 118.1, 54.8, 46.3, 30.9, 26.6. HRMS (MALDI-TOF) m/z : 1431.5755 [M^+]; calcd for $C_{100}H_{78}N_4O_4S$ [M^+]: 1431.5787.

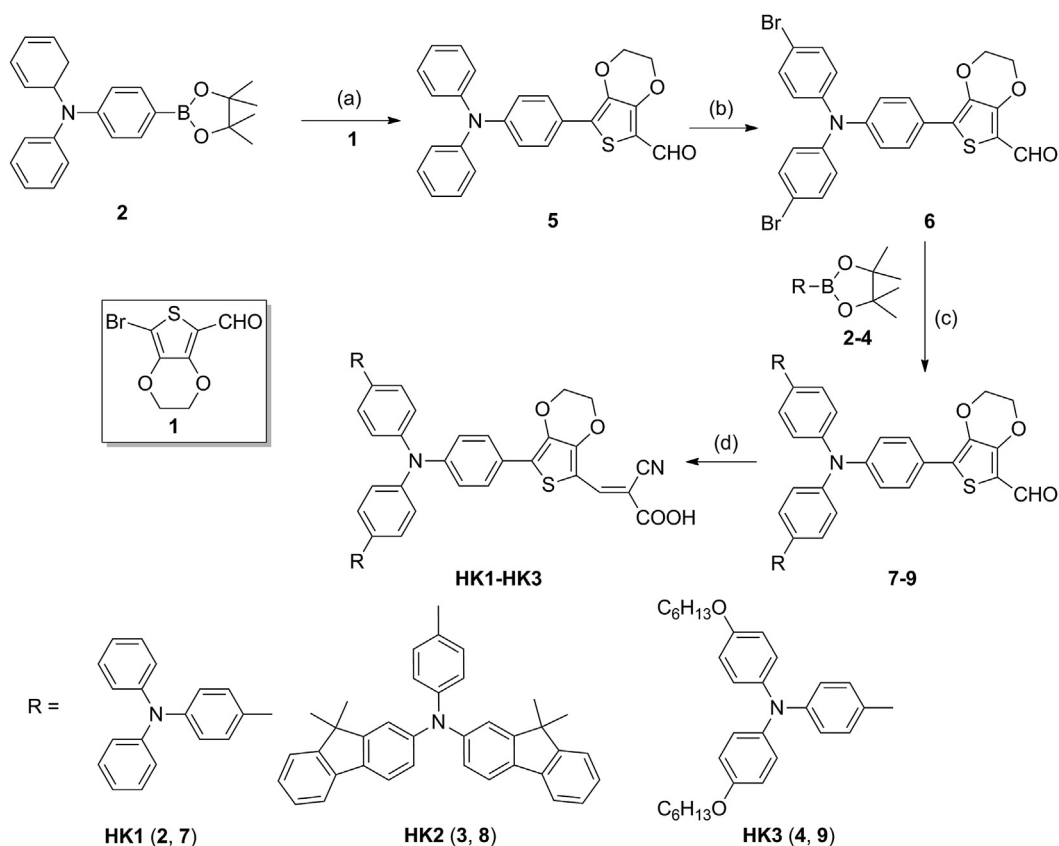
HK3: 1H NMR (400 MHz, d_6 -DMSO): δ (ppm) 8.08 (s, 1H), 7.64 (d, $J = 8.0$ Hz, 2H), 7.51 (d, $J = 8.0$ Hz, 4H), 7.41 (d, $J = 8.0$ Hz, 4H), 7.05 (t, $J = 8.0$ Hz, 6H), 6.97 (d, $J = 8.0$ Hz, 8H), 6.85 (d, $J = 8.0$ Hz, 8H), 6.76 (d, $J = 8.0$ Hz, 4H), 4.42 (s, 2H), 4.36 (s, 2H), 3.89 (m, $J = 6.4$ Hz, 8H), 1.38 (m, 9H), 1.27 (m, 18H), 1.14 (m, 5H), 0.83 (t, $J = 6.4$ Hz, 12H). ^{13}C NMR (400 MHz, d_6 -DMSO): δ (ppm) 154.3, 151.2, 151.0, 148.8, 143.1, 141.0, 140.5, 139.6, 135.0, 129.2, 128.1, 127.7, 127.1, 123.6, 122.9, 120.6, 119.9, 119.4, 54.8, 30.8, 28.8, 23.4, 21.8, 13.7. HRMS (MALDI-TOF) m/z : 1366.6779 [M^+]; calcd for $C_{88}H_{94}N_4O_8S$ [M^+]: 1366.6728.

2.2. Fabrication of dye-sensitized solar cells

A layer of ca. 5 μm TiO_2 film (13 nm paste, T/SP) was controlled on the FTO conducting glass by screen printing and then dried for 6 min at 125 $^{\circ}C$. This procedure was repeated two times (to prepare a thickness of ca. 10 μm) and the resulting surface was finally coated by a layer (ca. 4 μm) of TiO_2 paste (Ti-nanoxide 300) as the scattering layer. The tri-layer TiO_2 electrodes were gradually heated under an air flow at 275 $^{\circ}C$ for 5 min, 325 $^{\circ}C$ for 5 min, 375 $^{\circ}C$ for 5 min, 450 $^{\circ}C$ for 15 min, and 500 $^{\circ}C$ for 15 min. Then, these sintered films were soaked with 0.04 M $TiCl_4$ aqueous solution overnight at room temperature, washed with water and ethanol, further annealed at 450 $^{\circ}C$ for 30 min [30]. After the film was cooled to room temperature, it was immersed into a 5×10^{-4} M dye bath in CH_2Cl_2 solution and maintained in the dark for 24 h at room temperature. If chenodeoxycholic acid (CDCA) was used as a co-adsorbent, the TiO_2 film was soaked in a 20 mM CDCA bath in ethanol for 8 h and then in a 5×10^{-4} M dye bath in CH_2Cl_2 for 16 h at room temperature. The electrode was then rinsed with CH_2Cl_2 and dried. The size of the TiO_2 electrodes used was 0.25 cm^2 . To prepare the counter electrode, the Pt catalyst was deposited on cleaned FTO glass by spin coating with a drop of H_2PtCl_6 solution (0.02 M in 2-propanol solution) with heat treatment at 400 $^{\circ}C$ for 15 min. A hole (0.8 mm diameter) was drilled on the counter electrode using a drill press. The perforated sheet was cleaned with ultrasound in an ethanol bath for 15 min. The dye-covered TiO_2 electrode and Pt-counter electrode were assembled into a sandwich type cell and sealed with a hot-melt gasket of 25 mm thickness made of the ionomer Surlyn 1702 (DuPont). The electrolyte consisting of 0.6 M 1,2-dimethyl-3-propylimidazolium iodide (DMPiI), 0.1 M LiI, 0.05 M I_2 , and 0.5 M 4-*tert*-butylpyridine (TBP) in a mixture of acetonitrile and methoxypropionitrile (volume ratio, 7:3) was introduced into the cell via vacuum backfilling from the hole in the back of the counter electrode. At last, the hole was sealed by a film of Surlyn 1702 and a cover glass (0.1 mm thickness) using a heat sealer. The cell active area was tested with a mask, the size of which was about 1.5 mm larger than the side length of the TiO_2 electrode.

2.3. Characterization of dye-sensitized solar cells

The current–density voltage (J – V) characteristics of the DSSCs were measured by recording J – V curves using a Keithley 2400 source meter under the illumination of AM 1.5 G simulated solar light (Newport-91160 equipped with a 300 W Xe lamp and an AM 1.5 G filter). The incident light intensity was calibrated to 100 $mW\ cm^{-2}$ with a standard silicon solar cell (Newport 91150V). Action spectra of the incident monochromatic photon-to-electron conversion efficiency (IPCE) for the solar cells were obtained with



Scheme 1. Synthetic routes for three dyes **HK1–HK3**. (a) **1**, Pd(PPh₃)₄, 2 N K₂CO₃, THF, reflux; (b) NBS, THF; (c) Pd(PPh₃)₄, 2 N K₂CO₃, THF, reflux; (d) cyanoacetic acid, CH₃COOH, CH₃COONH₄, 120 °C.

a Newport-74125 system (Newport Instruments). The intensity of monochromatic light was measured with a Si detector (Newport-71640). The electrochemical impedance spectroscopy (EIS) measurements of all the DSSCs were performed using a Zahner IM6e Impedance Analyzer (ZAHNER-Elektrik GmbH & CoKG, Kronach, Germany). The frequency range is 0.10 Hz–100 kHz. The applied voltage bias is −0.70 V with a magnitude of the alternative signal of 10 mV.

2.4. Computational methods

To gain an insight into the molecular structure and electron distribution of the three dyes, density functional theory (DFT) and time-dependent density functional theory (TD-DFT) calculations were carried out with the Gaussian 03 package [31]. Molecular geometries were optimized at the Becke3LYP (B3LYP) level of DFT. TD-DFT was performed based on the optimized structures to obtain the excitation energies. The effective core potentials (ECPs) of Hay and Wadt with the double- ζ valence basis sets (LanL2DZ) were used to describe S atoms. The standard 6-31G basis set was used for all other atoms. Polarization functions were added for S(ζ d = 0.503).

3. Results and discussion

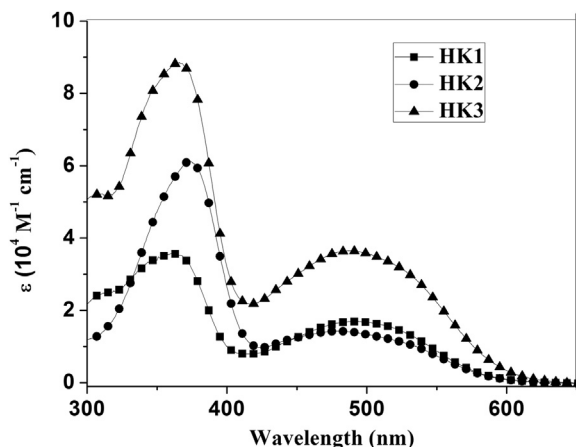
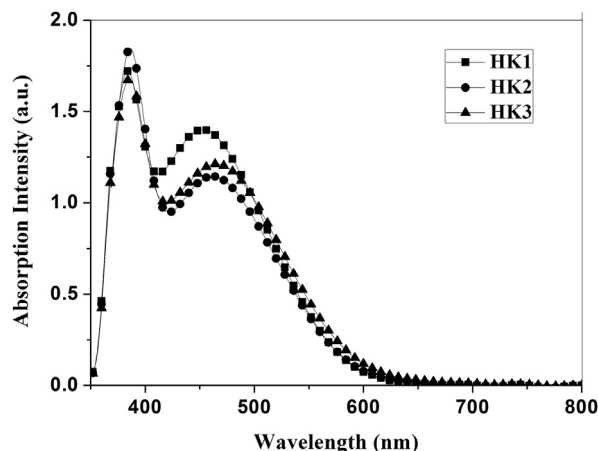
3.1. Synthesis and UV–visible absorption spectra

The synthetic protocol of the three dyes is depicted in Scheme 1. Bromination of compound **5** with NBS in THF gives dihalogenated intermediate **6**. Then, Suzuki coupling reaction between **6** and precursor **2**, **3** and **4** afford the aldehydes **7**, **8** and **9**, respectively. The corresponding carbaldehydes are finally converted to the target

organic photosensitizers (**HK1–HK3**) via the Knoevenagel condensation reactions.

The UV–visible absorption spectra of the three organic dyes **HK1**, **HK2** and **HK3** in CH₂Cl₂ solutions are shown in Fig. 2 and the spectroscopic parameters are also summarized in Table 1. The three dyes display two major absorption bands, appearing in the range of 300–400 nm and 420–620 nm, respectively. The former bands are ascribed to the localized aromatic π – π^* transitions and the later one can be assigned to the efficient intramolecular charge transfer transition (ICT) of the conjugated molecule with donor–acceptor nature. It is worth noting that the typical absorption peaks at around 370 nm for the three dyes are characteristic of very high molar extinction coefficients, **HK1** ($3.57 \times 10^4 \text{ M}^{-1} \text{ cm}^{-1}$ at 360 nm), **HK2** ($6.12 \times 10^4 \text{ M}^{-1} \text{ cm}^{-1}$ at 374 nm) and **HK3** ($8.85 \times 10^4 \text{ M}^{-1} \text{ cm}^{-1}$ at 366 nm), which can be attributed to the bulky dendritic triarylamine derivatives. For the ICT bands, the molar extinction coefficient of **HK3** ($3.65 \times 10^4 \text{ M}^{-1} \text{ cm}^{-1}$ at 488 nm) is higher than **HK1** ($1.70 \times 10^4 \text{ M}^{-1} \text{ cm}^{-1}$ at 489 nm) and **HK2** ($1.43 \times 10^4 \text{ M}^{-1} \text{ cm}^{-1}$ at 479 nm). It indicates that the introduction of the two hexyloxy groups on the outer triphenylamine units of the dendron in **HK1** can improve the extent of electron delocalization over the whole molecule and its light-harvesting ability, which is consistent with the observation in other similar studies [28].

When the organic dyes are adsorbed onto the TiO₂ films, the absorption spectra may show red-shift or blue-shift as compared to those in solutions due to the interaction between the dyes and the semiconductor surface. According to the previous studies, H-aggregation of the dye on TiO₂ surface might lead to the blue shift and J-aggregation to the red shift [32]. As shown in Fig. 3, the absorption spectra of **HK1–HK3** adsorbed on the surface of transparent

Fig. 2. Absorption spectra of HK1–HK3 in CH₂Cl₂ solution.Fig. 3. Normalized absorption spectra of HK1–HK3 on transparent TiO₂ films.

mesoporous TiO₂ films are similar to those in solutions. However, the absorption spectra of the dyes become broadened after adsorption on the TiO₂ films, which should favor the light harvesting of solar cells and enhance the photocurrent response region. The maximal absorption peaks for HK1–HK3 locate at 453, 461 and 465 nm, respectively. The UV–visible absorption peak is slightly blue-shifted by 36, 18 and 33 nm for HK1–HK3, respectively, when anchored at the TiO₂ surface as compared to the solution spectra due to the formation of dye H-aggregation on the TiO₂ surface or the interaction between the dyes and TiO₂. The emission maxima of the three dyes are found in the range of 500–750 nm, when excited at their respective absorption bands.

3.2. Electrochemical properties

To ensure the possibility of electron injection from the excited dye into the conduction band of TiO₂ and dye regeneration by I[−]/I₃[−] electrolyte, cyclic voltammetry (CV) have been performed in CH₂Cl₂ solution with 0.1 M ⁿBu₄NPF₆ as the supporting electrolyte, glassy carbon as a working electrode, Pt as a counter electrode, and Ag/AgCl (saturated KCl) as an internal reference electrode (Fig. 4). The examined HOMO and the LUMO levels are listed in Table 1. The estimated ground state oxidation potentials corresponding to the HOMO levels of HK1–HK3, calculated from the equation $E_{\text{HOMO}} = -(E_{\text{ox}} + 4.80)$ eV, are −5.24, −5.17, and −5.12 eV, respectively, which are in agreement with the order of the calculated HOMO energies (−4.82, −4.73 and −4.57 eV). The HOMO levels are sufficiently more negative than the I[−]/I₃[−] redox potential value (−4.95 eV), indicating a thermodynamic driving force for an

effective sensitizer regeneration process. Compared with HK2 and HK3, HK1 shows a more positive HOMO level, which results in a more efficient charge regeneration due to a larger energy gap. The band gap energies (E_{0-0}) of HK1–HK3 are 2.10, 1.95, and 1.80 eV, respectively, which can be estimated from the absorption onsets of the dyes adsorbed on the TiO₂ film. The LUMO levels for HK1–HK3, calculated from $E_{0-0} + E_{\text{HOMO}}$, are −3.02, −3.22, and −3.32 eV respectively, which are all much higher than the conduction band (CB) edge of TiO₂ (−4.4 eV), indicating that the electron injection process from the excited dye molecule to TiO₂ conduction band is energetically favorable. It is worthy noting that the LUMO energy level of HK1 is more positive than the conduction band of TiO₂ relative to HK2 and HK3, indicative of a more significant driving force for electron injection. These results clearly denote that the device performance of HK1 is superior to those of HK2 and HK3.

3.3. Molecular orbital calculations

Density functional theory (DFT) and time-dependent density functional theory (TD-DFT) calculations have been carried out with the Gaussian 03 package to further investigate the geometrical properties and electron density distribution of the frontier orbitals of the new dyes [31]. The ground state geometries of these three dyes were optimized at the hybrid Becke3LYP (B3LYP) level of DFT with the standard 6-31G (d) basis set. Molecular orbitals obtained

Table 1
Optical and electrochemical properties of HK1–HK3 dyes.

Dye	$\lambda_{\text{max}}^{\text{a}}/\text{nm}$ ($\epsilon \times 10^4 \text{ M}^{-1} \text{ cm}^{-1}$)	$\lambda_{\text{em}}^{\text{a}}/\text{nm}$	$\lambda_{\text{max}}^{\text{b}}/\text{nm}$	HOMO ^c /eV	E_{0-0}^{d} /eV	LUMO ^e /eV
HK1	489 (1.70), 360 (3.57)	627	453	−5.24	2.10	−3.02
HK2	479 (1.43), 374 (6.12)	620	461	−5.17	1.95	−3.22
HK3	488 (3.65), 366 (8.85)	625	465	−5.12	1.80	−3.32

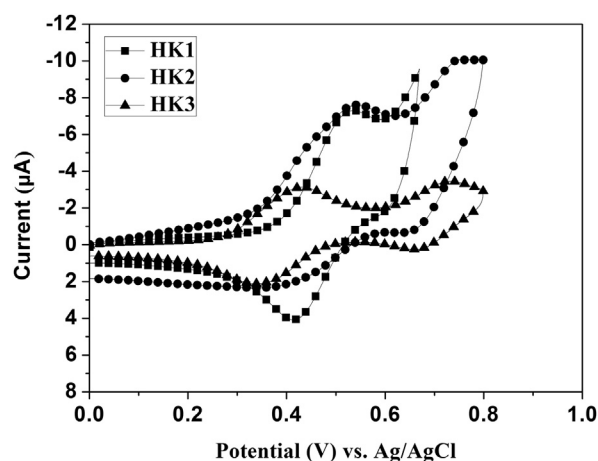
^a Absorption and emission maxima in CH₂Cl₂ with the concentration of $1 \times 10^{-5} \text{ mol L}^{-1}$.

^b Absorption maximum on the TiO₂ films.

^c HOMO energy level is derived by the CV method with 0.1 M (*n*-C₄H₉)₄NPF₆ as the supporting electrolyte (scanning rate, 100 mV s^{−1}; working electrode and counter electrode, Pt wires; reference electrode, Ag/AgCl).

^d E_{0-0} is estimated from the onset of the absorption spectrum.

^e LUMO energy level is calculated by the sum of E_{0-0} and HOMO energy level, $E_{\text{LUMO}} = E_{0-0} + E_{\text{HOMO}}$.

Fig. 4. Cyclic voltammetry (CV) measurement of HK1–HK3 in CH₂Cl₂ with 0.1 M ⁿBu₄NPF₆ used as the supporting electrolyte.

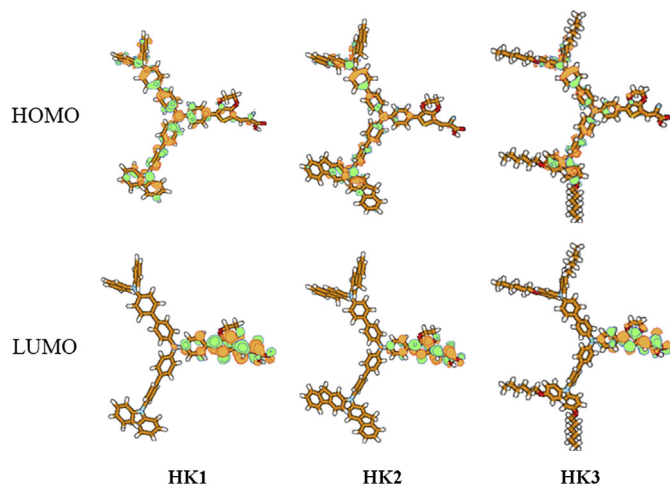


Fig. 5. Calculated HOMOs and LUMOs of HK1–HK3.

from the B3LYP calculations were plotted using the Molden 3.7 program written by Schaftenaar [33]. The calculated potential energy levels of HOMOs and LUMOs comply well with the experimental values of HOMO and LUMO estimated by CV. HK2 and HK3 have smaller HOMO–LUMO gaps (2.22 eV and 2.16 eV respectively) than HK1 (2.34 eV), which is consistent with the notion that electron-donating groups increase the HOMO energy and reduce the HOMO–LUMO gaps. As shown in Fig. 5, the electron density distribution of the HOMO for HK1–HK3 is mainly located at the dendritic triarylamine cores, whereas the electron density of the LUMO is primarily delocalized over the 3,4-ethylenedioxythiophene, cyanoacrylic acid acceptor unit and to a small extent at the neighboring *N*-substituted benzene. Both frontier orbitals provide sufficient overlap between the donor and the acceptor to guarantee a fast charge transition. Thus, excitation from the HOMO to the LUMO orbital by absorbing a photon should facilitate efficient photoinduced electron transfer from the electron-donating triarylamine derivatives to the conduction band of TiO₂ semiconductor via the terminal cyanoacrylic acid. Furthermore, all dihedral angles between triphenylamine units and benzene rings are all non-coplanar, which can help inhibit the close π – π aggregation effectively between the dyes molecule and enhance their thermal stability.

The transition probability was estimated by time-dependent density functional theory (TDDFT) with the B3LYP functional and the calculated oscillator strength (*f*) is shown in Table 2. The TDDFT results indicate that the wavelength required for the HOMO–LUMO transition (*S*₀ → *S*₁) is consistent with the magnitude of the HOMO–LUMO gaps measured in the solution.

3.4. Photovoltaic properties of DSSCs

The incident photon-to-current conversion efficiencies (IPCEs) of the DSSCs based on the three dyes were measured as shown in

Fig. 6. The onsets of the IPCE spectra for the three devices are significantly broadened and red-shifted as compared to the absorption spectrum of the dyes absorbed on TiO₂. The IPCE curves for HK1–HK3 show a broad absorption in the range of 300–700 nm with the maximum values of 62%, 58% and 46% respectively, whereas in the long wavelength region HK1 show a little higher value than HK2 and HK3 that may be ascribed to its high electron injection efficiency. The IPCE spectra of these dyes are consistent with their absorption spectra when adsorbed onto the TiO₂ film.

The short-circuit photocurrent density (*J*_{sc}), open-circuit photovoltage (*V*_{oc}), and fill factor (*ff*) of the DSSCs based on the three dyes were measured under standard AM 1.5G sunlight illumination. The photocurrent–voltage (*J*–*V*) curves of these dyes are shown in Fig. 7 and detailed photovoltaic parameters are listed in Table 3. The HK1 sensitized solar cells shows the highest PCE of 5.11% (*J*_{sc} = 10.41 mA cm^{−2}, *V*_{oc} = 0.76 V, *ff* = 0.65). The short-circuit photocurrent values for the three dyes are in the order of HK1 > HK2 > HK3 which is in agreement with the order of IPCE values. The results are consistent with the electron injection efficiency and the appropriate energy band gap of the three dyes. The devices based on the three dyes show quite high *V*_{oc}, especially that of HK1 (up to 760 mV), which might be related to the presence of the secondary bulky electron-donating groups. It is noticeable that the molar extinction coefficient of HK1 is lower than that of HK2 and HK3, although the three dyes have similar structures, however, HK1 exhibits the best photovoltaic performance with higher *J*_{sc} and *V*_{oc} values. The essential reason may be that HK2 and HK3 with bigger bulky three-dimensional structural electron-donating groups may produce steric hindrance to self-assemble the dyes on the TiO₂ surface, resulting in lower efficiencies of surface coverage and electron injection, and subsequently lower photovoltaic performance DSSCs relative to HK1 [34].

Generally, for most organic dyes suffering from aggregation, co-adsorption of CDCA can increase the photovoltaic performance significantly because it can occupy the surface site of TiO₂ by its carboxyl group and compete with the sensitizers to hinder the unfavorable dye aggregation, which cause intermolecular energy transfer and sequentially result in the excited-state quenching of the dyes [35,36]. In order to further probe the effect of configuration of the sensitizers with the bulky dendritic triarylamine derivatives as the donor on prohibiting dye aggregation, the co-adsorption strategy was applied by adding chenodeoxycholic acid (CDCA) during the sensitization process. Fig. 7 shows the photovoltaic performances of DSSCs based on HK1–HK3 with or without the addition of 20 mM CDCA and the detailed data are also summarized in Table 3. It was found that, the *J*_{sc} of these dyes dramatically decreased by about 10% with the addition of CDCA, whereas *V*_{oc} and *ff* remained almost the same. Correspondingly, the IPCE curves combined in Fig. 6 for HK1–HK3 together with 20 mM CDCA show a similar broad absorption in the same range of 300–700 nm with a lower maximum value of 56%, 50% and 41%, respectively. And the IPCE values of HK1–HK3 without or with the addition of CDCA are well consistent with the *J*_{sc} values from the *J*–*V* curves, which nicely correlates with the fact that the IPCE

Table 2
TD-DFT calculation results of the three compounds.

Compound	The largest coefficient in the CI expansion of the <i>T</i> ₁ state ^a (<i>S</i> ₀ → <i>T</i> ₁ excitation energy)	The largest coefficient in the CI expansion of the <i>S</i> ₁ state ^a (<i>S</i> ₀ → <i>S</i> ₁ excitation energy)	The oscillator strength (<i>f</i>) of the <i>S</i> ₀ → <i>S</i> ₁ transition
HK1	H → L: 0.52 (766.8 nm)	H → L: 0.68 (584.3 nm)	0.5245
HK2	H → L: 0.50 (771.4 nm)	H → L: 0.69 (613.5 nm)	0.3445
HK3	H → L: 0.47 (783.6 nm)	H → L: 0.69 (634.0 nm)	0.3304

CI stands for configuration interaction.

^a H → L represents the HOMO to LUMO transition.

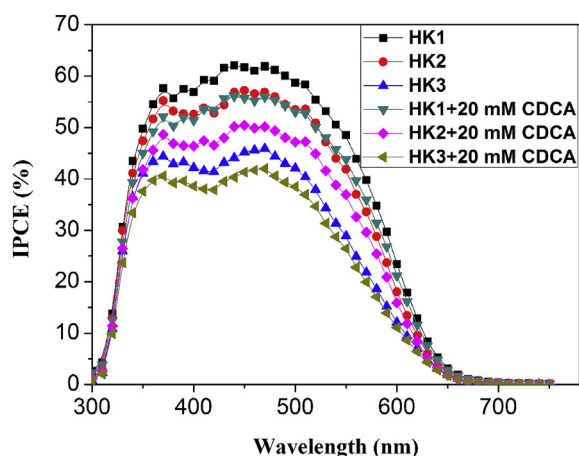


Fig. 6. The IPCE spectrum for the DSSCs sensitized by HK1–HK3 with or without 20 mM CDCA.

value corresponds to the photocurrent density produced in the external circuit under monochromatic illumination of the cell divided by the photon flux that strikes the cell [37]. The results indicate that CDCA is not beneficial for these sensitizers to improve the photovoltaic performance. And the main possible explanation is that a large amount of the co-adsorption of CDCA with dyes on the TiO_2 surface decreases the adsorption amount of these dyes, resulting in a loss of light harvesting and then a lower efficiency of the electron injection into the TiO_2 conduction band. In other words, these sensitizers with the introduction of bulky dendritic triarylamine derivatives as donors would not aggregate on the TiO_2 surface in the absence of co-adsorbent CDCA. We have also performed the experiments with thicker TiO_2 , and the results indicate that the increase in thickness leads to higher recombination probability due to the prolonged electron path length, corresponding to a poor DSSC performance.

3.5. Electrochemical impedance spectroscopy analysis

Electrochemical Impedance Spectroscopy (EIS) technique was also used to elucidate the interfacial charge recombination process in DSSCs based on the HK1–HK3 dyes under a forward bias of -0.7 V in the dark from 0.1 Hz to 100 kHz, which provided some valuable information for understanding the photovoltaic findings

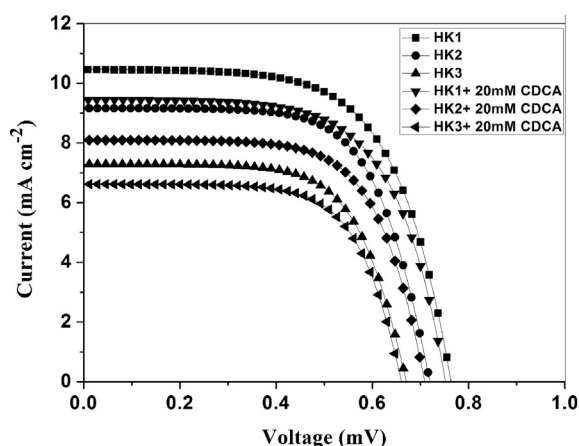


Fig. 7. The J – V performance for the DSSCs sensitized by HK1–HK3 with or without 20 mM CDCA.

Table 3

Photovoltaic performance of DSSCs using dyes HK1–HK3 with or without 20 mM CDCA.^a

Dye	CDCA ^b	J_{sc} (mA cm^{-2})	V_{oc} (V)	ff	η (%)
HK1	0	10.41	0.76	0.65	5.11
	20 mM	9.40	0.75	0.65	4.61
HK2	0	9.15	0.72	0.67	4.42
	20 mM	8.07	0.71	0.68	3.90
HK3	0	7.30	0.67	0.68	3.34
	20 mM	6.60	0.66	0.70	3.05
N719	0	16.10	0.69	0.67	7.47

^a Illumination: 100 mW cm^{-2} simulated AM 1.5 G solar light; electrolyte containing: 0.1 M LiI + 0.05 M I_2 + 0.6 M DMPII + 0.5 M TBP in the mixed solvent of acetonitrile and 3-methoxypropionitrile (7:3, v/v).

^b Exposed to 20 mM CDCA solution for 6 h before the sensitizer bath.

above [38]. In addition, some important parameters were obtained by fitting the EIS spectra with an equivalent model [39]. R_s , R_{rec} , and R_{CE} represent the series resistance, charge-transfer resistances at the dye/ TiO_2 /electrolyte interface and counter electrode (CE),

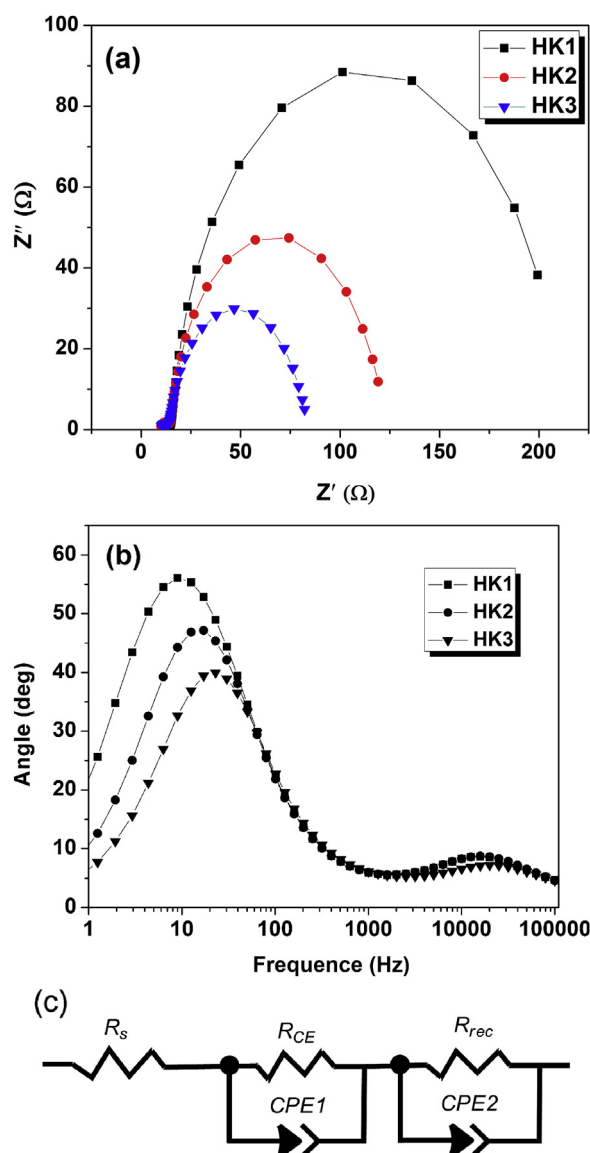


Fig. 8. (a) EIS Nyquist plots and (b) EIS Bode plots and (c) equivalent circuits were used to fit the impedance spectra of DSSCs based on the dyes HK1–HK3.

Table 4

Parameters obtained by fitting the EIS spectra of **HK1**–**HK3** sensitized DSSCs using the equivalent circuit.^a

Dye	R_s [Ωcm^{-2}]	R_{rec} [Ωcm^{-2}]	R_{CE} [Ωcm^{-2}]	τ_e [ms]
HK1	11.5	210.2	5.0	18.3
HK2	10.2	82.7	4.5	13.2
HK3	10.7	63.7	3.8	9.6

^a The reaction resistance of DSSCs consisting of $\text{TiO}_2/\text{dye}/\text{electrolyte}$ and $\text{Pt}/\text{electrolyte}$ interface based on **HK1**–**HK3** were analyzed by the software (ZsimpWin) using an equivalent circuit.

respectively. The R_s and R_{CE} corresponding to the first semicircle in the Nyquist plots (Fig. 8a) show almost the same values in the three DSSCs because of the same electrode material and electrolyte used. And the R_{rec} corresponding to the larger semicircle were tested by software (ZsimpWin) with an equivalent circuit (Fig. 8c). As shown in Table 4, the R_{rec} of the **HK1**–**HK3** dyes are 210.2, 82.8, and $63.7\ \Omega\ \text{cm}^{-1}$, respectively, which are expected to result in the enhanced injected electron recombination resistance in the order **HK3** < **HK2** < **HK1**, as well as substantially increasing photocurrents and photovoltages in the same order. The results deduced here are well consistent with the trend of the J_{sc} and V_{oc} values observed for the three dyes based cells.

From the EIS measurements, the electron lifetime (τ_e) expressing the electron recombination between the electrolyte and TiO_2 can be extracted from the angular frequency (ω_{rec}) at the mid-frequency peak in the Bode phase plots (Fig. 8b) using the Equation (1), in which f is the corresponding frequency of the peak [40].

$$\tau_e = 1/\omega_{\text{rec}} = 1/2\pi f \quad (1)$$

Estimated from above equation, the electron lifetimes of the **HK1**–**HK3** dyes are 18.3, 13.2, and 9.6 ms, respectively, likewise supporting the observed shift in the V_{oc} value. The relatively longer electron lifetimes indicate that introduction of the bulky triarylamine dendritic derivatives as donors can effectively block the charge recombination to gain better performance in J_{sc} and V_{oc} values. As expected, the sequence of the electron lifetimes is well in agreement with those observed for the photovoltaic parameters. In other words, the longer electron lifetime and larger charge recombination resistance may be the main reason for the highest V_{oc} (0.76 V) and J_{sc} ($10.41\ \text{mA cm}^{-2}$) values in the DSSC based on **HK1**.

4. Conclusions

In summary, we have designed and synthesized three new organic photosensitizers **HK1**–**HK3**, with dendritic triarylamine derivatives as the electron donor, 3,4-ethylenedioxythiophene (EDOT) as the linker and cyanoacrylic acid as the acceptor moiety. The cell based on **HK1** exhibits a PCE of 5.11% without the co-adsorbent CDCA, which is higher than that of **HK2** (4.42%) and **HK3** (3.34%) under AM 1.5G sunlight. Moreover, the PCEs of DSSCs are significantly decreased by about 9.7% in the presence of the co-adsorbent CDCA. The results indicate that the non-planar bulky electron-donating groups in these dye molecules can effectively suppress the aggregation of the dye molecules and improve the photovoltaic performance in the absence of the co-adsorbent. In the future, via combination of experimental and theoretical approaches, we are going to further optimize the chemical structure of the dyes by employing oligothiophene as the bridge and further extending the π -conjugation of the chromophore, with an aim to figure out the balance between the inhibition of aggregation and high performance of the co-adsorbent-free DSSCs.

Acknowledgments

We thank Hong Kong Research Grants Council (HKBU202210, HKBU202811 and HKBU203011) and Hong Kong Baptist University (FRG2/09–10/058, FRG2/10–11/101, FRG2/11–12/007, FRG2/10–11/101 and IRACE/11–12/04) for the financial support. W.-K.W. and W.-Y.W. also thank a grant from Areas of Excellence Scheme, University Grants Committee, Hong Kong (Project No. [AoE/P-03/08]). W.-Y.W. thanks Prof. He Tian at the East China University of Science and Technology for the collaboration and the National Natural Science Foundation of China (NSFC) (project number: 21029001) for financial support. X.Z. also thanks the financial support from The Science, Technology and Innovation Committee of Shenzhen Municipality (JCYJ20120615155451326).

References

- [1] (a) B. O'Regan, M. Grätzel, *Nature* 353 (1991) 737–740; (b) A. Hagfeldt, M. Grätzel, *Chem. Rev.* 95 (1995) 49–68.
- [2] M. Grätzel, *Acc. Chem. Res.* 42 (2009) 1788–1798.
- [3] M. Grätzel, *Nature* 414 (2001) 338–344.
- [4] N. Robertson, *Angew. Chem. Int. Ed.* 118 (2006) 2398–2402.
- [5] M. Pagliaro, G. Palmisano, R. Ciriminna, V. Lodo, *Energy Environ. Sci.* 115 (2009) 838–844.
- [6] P. Wang, B. Wenger, R. Humphry-Baker, J.E. Moser, J. Teuscher, W. Kanteleher, J. Mezger, E.V. Stoyanov, S.M. Zakeeruddin, M. Grätzel, *J. Am. Chem. Soc.* 127 (2005) 6850–6856.
- [7] M.K. Nazeeruddin, A. Kay, I. Rodicio, R. Humphry-Baker, E. Muller, P. Liska, N. Vlachopoulos, M. Grätzel, *J. Am. Chem. Soc.* 115 (1993) 6382–6390.
- [8] (a) M.K. Nazeeruddin, F.D. Angelis, S. Fantacci, A. Selloni, G. Viscardi, P. Liska, S. Ito, B. Takeru, M. Grätzel, *J. Am. Chem. Soc.* 127 (2005) 16835–16847; (b) M.K. Nazeeruddin, R. Splivallo, P. Liska, P. Comte, M. Grätzel, *Chem. Commun.* 12 (2003) 1456–1457.
- [9] (a) M.K. Nazeeruddin, P. Péchy, T. Renouard, S.M. Zakeeruddin, R. Humphry Baker, P. Comte, P. Liska, L. Cevey, E. Costa, V. Shklover, L. Spiccia, G.B. Deacon, C.A. Bignozzi, M. Grätzel, *J. Am. Chem. Soc.* 123 (2001) 1613–1624; (b) Y. Chiba, A. Islam, Y. Watanabe, R. Komiya, N. Koide, L. Han, *Jpn. J. Appl. Phys.* 45 (2006) L638–L640; (c) M.K. Nazeeruddin, P. Péchy, M. Grätzel, *Chem. Commun.* 18 (1997) 1705–1706.
- [10] K. Hara, T. Sato, R. Katoh, A. Furube, Y. Ohga, A. Shinpo, S. Suga, K. Sayama, H. Sayama, H. Sugihara, H. Arakawa, *J. Phys. Chem. B* 107 (2003) 597–606.
- [11] N. Koumura, Z. Wang, S. Mori, M. Miyashita, E. Suzuki, K. Hara, *J. Am. Chem. Soc.* 128 (2006) 14256–14257.
- [12] Y. Cao, Y. Bai, Q.J. Yu, Y.M. Cheng, S. Liu, D. Shi, F. Gao, P. Wang, *J. Phys. Chem. C* 112 (2008) 6290–6297.
- [13] W. Xu, J. Pei, J.F. Shi, S.J. Peng, J. Chen, *J. Power Sources* 183 (2008) 792–798.
- [14] J. Tang, W.J. Wu, J.L. Hua, J. Li, X. Li, H. Tian, *Energy Environ. Sci.* 2 (2009) 982–990.
- [15] C. Teng, X.C. Yang, S.F. Li, M. Cheng, A. Hagfeldt, L.Z. Wu, L.C. Sun, *Chem. Eur. J.* 16 (2010) 13127–13138.
- [16] M. Liang, M. Lu, Q.L. Wang, W.Y. Chen, H.Y. Han, Z. Sun, S. Xue, *J. Power Sources* 196 (2011) 1657–1664.
- [17] Y. Cui, Y.Z. Wu, X.F. Lu, X. Zhang, G. Zhou, F.B. Miapeli, W.H. Zhu, Z.S. Wang, *Chem. Mater.* 23 (2011) 4394–4401.
- [18] Y.C. Chen, Y.H. Chen, H.H. Chou, S. Chaurasia, Y.S. Wen, J.T. Lin, C.F. Yao, *Chem. Asian J.* 7 (2012) 1074–1084.
- [19] (a) M. Velusamy, K. Thomas, J.T. Lin, Y.C. Hsu, K.C. Ho, *Org. Lett.* 7 (2005) 1899–1902; (b) R. Chen, X. Yang, H. Tian, X. Wang, A. Hagfeldt, L. Sun, *Chem. Mater.* 19 (2007) 4007–4015.
- [20] D.P. Hagberg, T. Marinado, K.M. Karlsson, K. Nonomura, P. Qin, G. Boschloo, T. Brinck, A. Hagfeldt, L. Sun, *J. Org. Chem.* 72 (2007) 9550–9556.
- [21] D. Liu, R.W. Fessenden, G.L. Hug, P.V. Kamat, *J. Phys. Chem. B* 101 (1997) 2583–2590.
- [22] S. Kim, J.K. Lee, S.O. Kang, J. Ko, J.H. Yum, S. Frantacci, F.D. Angelis, D.D. Censo, M.K. Nazeeruddin, M. Grätzel, *J. Am. Chem. Soc.* 128 (2006) 16701–16707.
- [23] Z.J. Ning, Q. Zhang, W.J. Wu, H.C. Pei, B. Liu, H. Tian, *J. Org. Chem.* 73 (2008) 3791–3797.
- [24] S. Paek, H. Choi, C.W. Lee, M.S. Kang, K. Song, M.K. Nazeeruddin, J. Ko, *J. Phys. Chem. C* 114 (2010) 14646–14653.
- [25] Z.Q. Wan, C.Y. Jia, J.Q. Zhang, Y.D. Duan, Y. Lin, Y. Shi, *J. Power Sources* 199 (2012) 426–431.
- [26] L. Wang, H.Y. Wang, H.H. Fang, H. Wang, Z.Y. Yang, B.R. Gao, Q.D. Chen, W. Han, H.B. Sun, *Adv. Funct. Mater.* 22 (2012) 2783–2791.
- [27] W.H. Liu, I.C. Wu, C.H. Lai, P.T. Chou, Y.T. Li, C.L. Chen, Y.Y. Hsu, Y. Chi, *Chem. Commun.* 41 (2008) 5152–5154.
- [28] R.Z. Li, J.Y. Liu, N. Cai, M. Zhang, P. Wang, *J. Phys. Chem. B* 114 (2010) 4461–4464.

- [29] J. Zhang, F.C. Zhao, X.J. Zhu, W.K. Wong, D.G. Ma, W.Y. Wong, *J. Mater. Chem.* 22 (2012) 16448–16457.
- [30] C.J. Barbé, F. Arendse, P. Comte, M. Jirousek, F. Lenzmann, V. Shklover, M. Grätzel, *J. Am. Ceram. Soc.* 80 (1997) 3157–3171.
- [31] M.J. Frisch, et al., Gaussian 03, Revision E01, Gaussian, Inc., Pittsburgh, PA, 2003.
- [32] F.R. Dai, Y.C. Chen, L.F. Lai, W.J. Wu, C.H. Cui, G.P. Tan, X.Z. Wang, J.T. Lin, H. Tian, W.Y. Wong, *Chem. Asian J.* 7 (2012) 1426–1434.
- [33] G. Scheefenaar, Molden v3.7; CAOS/CAMM Center Nijmegen: Toernooiveld, Nijmegen, Netherlands, 2001.
- [34] X. Jiang, T. Marinado, E. Gabrielsson, D.P. Hagberg, L.C. Sun, A. Hagfeldt, *J. Phys. Chem. C* 114 (2010) 2799–2805.
- [35] Z.S. Wang, Y. Cui, Y. Dan-oh, C. Kasada, A. Shinpo, K. Hara, *J. Phys. Chem. C* 111 (2007) 7224–7230.
- [36] P. Wang, S.M. Zakeeruddin, S.P. Comte, R. Charvet, R. Humphrybaker, M. Grätzel, *J. Phys. Chem. B* 107 (2003) 14336–14341.
- [37] A. Hagfeldt, G. Boschloo, L.C. Sun, L. Kloo, H. Pettersson, *Chem. Rev.* 110 (2010) 6595–6663.
- [38] D.B. Kuang, S. Uchida, R. Humphry-Baker, S.M. Zakeeruddin, M. Grätzel, *Angew. Chem. Int. Ed.* 47 (2008) 1923–1927.
- [39] N. Koide, A. Islam, Y. Chiba, L.Y. Han, *J. Photochem. Photobiol. A* 182 (2006) 296–305.
- [40] (a) J.A. Mikroyannidis, P. Surech, M.S. Roy, G.D. Sharma, *Electrochim. Acta* 56 (2011) 5616–5623;
(b) L.Y. Lin, C.H. Tsai, K.T. Wong, T.W. Huang, L. Hsieh, S.H. Liu, H.W. Lin, C.C. Wu, S.H. Chou, S.H. Chen, A.I. Tsai, *J. Org. Chem.* 75 (2010) 4778–4785.